Environmental Science and Ecotechnology 14 (2023) 100236

Contents lists available at ScienceDirect

Environmental Science and Ecotechnology

journal homepage: www.journals.elsevier.com/environmental-science-and-ecotechnology/

Original Research

Post-synthetic thiol modification of covalent organic frameworks for mercury(II) removal from water

Wei Wang [a], Minjuan Gong [a], Donghai Zhu [a], Mohammadtaghi Vakili [b], Zahra Gholami [b], Huanhuan Jiang [a], Shuangxi Zhou [a, **], Han Qu [c, *]

[a] State Key Laboratory of Plateau Ecology and Agriculture, Qinghai University, Xi'ning, Qinghai Province, 810016, China
[b] ORLEN UniCRE, a.s, Revoluční 1521/84, 400 01, Ústí nad Labem, Czech Republic
[c] Key Laboratory of the Three Gorges Region's Eco-Environment, Ministry of Education, College of Environment and Ecology, Chongqing University, Chongqing, 400044, China

ARTICLE INFO

Article history:
Received 7 September 2022
Received in revised form
3 January 2023
Accepted 3 January 2023

Keywords:
Covalent organic frameworks
Post-modification
Hg(II)
Density functional theory calculation
Synergistic adsorption mechanism

ABSTRACT

Various materials have been developed for environmental remediation of mercury ion pollution. Among these materials, covalent organic frameworks (COFs) can efficiently adsorb Hg(II) from water. Herein, two thiol-modified COFs (COF-S-SH and COF-OH-SH) were prepared, through the reaction between 2,5-divinylterephthalaldehyde and 1,3,5-tris-(4-aminophenyl)benzene, followed by post-synthetic modification using bis(2-mercaptoethyl) sulfide and dithiothreitol, respectively. The modified COFs showed excellent Hg(II) adsorption abilities with maximum adsorption capacities of 586.3 and 535.5 mg g^{-1} for COF-S-SH and COF-OH-SH, respectively. The prepared materials showed excellent selective absorbability for Hg(II) against multiple cationic metals in water. Unexpectedly, the experimental data showed that both co-existing toxic anionic diclofenac sodium (DCF) and Hg(II) performed positive effect for capturing another pollutant by these two modified COFs. Thus, a synergistic adsorption mechanism between Hg(II) and DCF on COFs was proposed. Moreover, density functional theory calculations revealed that synergistic adsorption occurred between Hg(II) and DCF, which resulted in a significant reduction in the adsorption system's energy. This work highlights a new direction for application of COFs to simultaneous removal of heavy metals and co-existing organic pollutants from water.

1. Introduction

Pollution of aquatic environments with heavy metals is a serious issue. Mercury ions [Hg(II)] are highly bioaccumulative and toxic [1]. Exposure to Hg(II) can cause eye, muscle, and skin damage, dermatitis, and kidney, liver, heart, and central nervous system damage [2,3]. There have been significant efforts to effectively remove mercury from aqueous environment [4–6]. Among the numerous techniques for this purpose, adsorption is a promising method to address this environmental challenge [6,7]. However, the application of conventional adsorbents such as activated carbon [8], clay [9], hydrated lime [10], and biosorbents [11] is limited because they have low Hg(II) adsorption capacities and selectivity. Therefore, suitable adsorbents need to be developed with fast kinetics, high adsorption capacities, and excellent selectivity for effective removal of Hg(II) from aqueous solutions.

The concept of covalent organic frameworks (COFs) has broadened the business of adsorbents for the distinct nature of tunable building blocks by pre-designing porous topology skeletons [12–15]. Over the past decades, COFs with different roles, e.g., semiconductors [16–19], and in energy conversion and storage [20–24], medical [25–27], and environmental applications [28–31].

COFs can be modified with specific functional groups that are incorporated in the monomers or introduced into the COFs matrix to improve the adsorption capacity and selectivity for pollutant removal [32]. For instance, the addition of quaternary ammonium cations and hydroxyl groups improves the ability of COFs to absorb harmful pollutants such as perfluorooctanoic acid [33] and Cr(VI) [34] from water. Functional groups such as methyl sulfide [35],

* Corresponding author.
** Corresponding author.
E-mail addresses: zhoushuangxi_qhu@163.com (S. Zhou), quhancau@gmail.com (H. Qu).

https://doi.org/10.1016/j.ese.2023.100236

dithiol [36], and thio groups [37] in COFs show excellent binding abilities for Hg(II) ions. Although these prepared COFs perform well for Hg(II) removal, the effects of co-existing contaminants have not been investigated, and the interactions between Hg(II) ions and co-contaminants during adsorption are not clear. For instance, as the typical component of COFs, the benzene ring can easily adsorb aromatic organic compounds via π-π interaction [38], especially for anionic organic substances, which could be adsorbed by COFs modified aromatic imines with electrophilic N through hydrogen bonds or electrostatic interaction [31]. In addition, the role of the surface charge and number of functional groups in removal of co-existing anionic organic substances might be non-negligible [39]. Consequently, it will be interesting to investigate whether adsorbed cationic Hg(II) or anionic contaminants promote or inhibit the adsorption of co-existing oppositely charged substances. Thus, an understanding of the adsorption behavior between anionic ions and Hg(II) in the presence of coexistence substances will help reveal the mechanism of metal adsorption.

In this study, 2,5-divinylterephthalaldehyde (Dva) and 1,3,5-tris-(4-aminophenyl)benzene (Tab) were used as monomers to synthesize the matrix of COF-V via a Schiff base reaction. Then, the exposed vinyl groups in COF-V were further modified by bis(2-mercaptoethyl) sulfide and dithiothreitol to obtain functionalized COF-S-SH and COF-OH-SH, respectively. The post-synthetically thiol-modified COFs were characterized, and their abilities to adsorb Hg(II) from aqueous media were investigated. To investigate the function of the adsorbed Hg(II), anionic diclofenac sodium (DCF) was introduced into the adsorption system. The interactions between Hg(II) and anionic DCF were studied, including the adsorption behavior and mechanism of Hg(II), and the effect of co-existing anionic organic pollutant. Finally, the reusability of the two functionalized COFs for Hg(II) removal was evaluated.

2. Materials and methods

2.1. Chemicals and materials

Mercury(II) nitrate and acetone were purchased from Sinopharm Chemical Reagent Co., Ltd. (Beijing, China). Bis(2-mercaptoethyl) sulfide, diclofenac sodium (DCF), DL-dithiothreitol, tetrahydrofuran, acetic acid, 1,2-dichlorobenzene, *n*-butanol, azobisisobutyronitrile (AIBN), and *N*,*N*-dimethylformamide were obtained from Shanghai Aladdin Biochemical Technology Co., Ltd. (Shanghai, China). 2,5-Divinylterephthalaldehyde (Dva) and 1,3,5-tris-(4-aminophenyl)benzene (Tab) were obtained from Jilin Chinese Academy of Sciences-Yanshen Technology Co., Ltd. (Jilin, China). Ultrapure water was produced using a Milli-Q water purification system (Millipore, USA). All of the chemicals were of analytical grade.

2.2. COFs preparation

2.2.1. Synthesis of COF-V

According to the previous report [36], 2,5-divinylterephthalaldehyde and 1,3,5-tris-(4-aminophenyl)benzene were dispersed in a mixture of 1,2-dichlorobenzene and *n*-butanol. The two solutions were then mixed in a glass tube, and the certain acetic acid (6 mol L^{-1}) was slowly added to the mixture. The product was washed by Soxhlet extraction with tetrahydrofuran for three days and then dried under vacuum at 50 °C to obtain COF-V.

2.2.2. Synthesis of COF-S-SH and COF-OH-SH

COF-V (40 mg), azobis(isobutyronitrile) (4 mg), and 0.5 mM bis(2-mercaptoethyl) sulfide (or dithiothreitol) were mixed in a 50 mL Schlenk tube under N_2 atmosphere at 80 °C for 48 h. The precipitates were washed by tetrahydrofuran and acetone for two times, respectively. The products synthesized by bis(2-mercaptoethyl) sulfide and dithiothreitol were dried at 50 °C under vacuum and named COF-S-SH and COF-OH-SH, respectively.

2.3. Characterization of the COFs

The X-ray diffraction (XRD) patterns of COFs were obtained using an X-ray diffractometer (Rigaku S2) equipped with a Cu-Kα radiation source (λ = 0.154 nm). The surface morphologies of prepared COFs were observed by scanning electron microscopy (SEM, JSM-6460LV, JEOL). A gas adsorption instrument (Autosorb iQ, Quantachrome Corp.) was used to measure the specific surface area and pore size distribution by nitrogen adsorption at 77 K. FTIR spectra of the prepared COFs were measured by a Fourier transform infrared spectrometer (PerkinElmer). An X-ray photoelectron spectroscopy (XPS, Kratos AXIS SUPRA™, Shimadzu) was used to record the XPS spectra of prepared COFs and the composite after Hg(II) adsorption. An elemental analyzer (EA3000, ELTRA) was used to determine the elemental compositions of the COFs.

2.4. Adsorption and recycle experiments

To evaluate the adsorption performance of prepared COFs, batch experiments were conducted on a shaker (180 rpm) at room temperature (25 °C) for a specific time. Kinetic experiments were carried out in conical flasks containing 100 mL of 2 mg L^{-1} Hg(II) solution. The initial concentration of Hg(II) ranged from 5 to 200 mg L^{-1} and the adsorption isotherm tests were performed under 2.5 mg COFs in a 50 mL solution. The effect of the solution pH on Hg(II) adsorption was also studied in the range of 2−8. The pH was adjusted by 1 M HCl or NaOH in a bottle containing the adsorbents (50 mg L^{-1}) and 50 mL Hg(II) solution (2 mg L^{-1}). The adsorption selectivity was tested in a mixed solution containing nine cationic ions (K^+, Na^+, Ca^{2+}, Mg^{2+}, Pb^{2+}, Cd^{2+}, Cu^{2+}, Mn^{2+}, and Zn^{2+}), whose molar quantity were equal to Hg(II). Co-adsorption kinetic experiments were conducted in a mixture solution containing Hg(II) and DCF (0.01 mmol L^{-1}). To further explore the co-adsorption mechanism between Hg(II) and DCF on COFs, one adsorbate was pre-adsorbed by COFs for 30 min, and then another adsorbate was added to make it a bisolute system with a concentration of 0.01 mmol L^{-1} for both substances. An atomic fluorescence spectrometer (AFS-933, Titan) and inductively coupled plasma optical emission spectrometer (ICP-OES, Thermo) were used to detect the concentrations of Hg(II) and other co-existing cationic ions, respectively.

A conical flask containing 2 mg L^{-1} Hg(II) and 50 mg L^{-1} COFs was used for the recyclability test. The used COFs were then collected using a filter membrane, submerged in HCl solution (0.75 M) for 3 h, and then washed with deionized water to desorb Hg(II). The regenerated COFs were used for the next cycle under the same adsorption conditions.

2.5. Computational methods

Gaussian software was used to perform theoretical calculations [40]. To obtain the optimal geometries of Hg(II), DCF and their adsorption conjugate, geometry optimization and frequency calculations were calculated with the PBE0 functional and the def2-SVP basis set [41]. To further improve the accuracy of the analysis, the DFT-D3 dispersion correction with BJ damping was adopted to correct the weak interaction [42,43]. Single point energy calculations were performed with a larger def2-TZVP basis set [44,45]. The SMD implicit solvation model was applied to account for the solvent effects of water [46].

3. Results and discussion

3.1. Preparation and characterization of COFs

As shown in Fig. 1 (the synthetic scheme), the vinyl groups were designed for post-synthetic modification linking of the -OH-SH and -S-SH groups through the thiol-ene "click" reaction in the presence of AIBN and under nitrogen [35]. The XPS and elemental analysis results both confirmed the proposed reaction worked as intended. As shown in Fig. S1a, S peaks of COF-S-SH and COF-OH-SH in the XPS survey indicated the thiol-ene "click" reaction was successfully executed. Moreover, the content of S was higher in COF-S-SH and COF-OH-SH than in COF-V (Fig. 2d and Table S1). The O element was only detected in COF-OH-SH, which further affirmed the successful introduction of -OH-SH. According to the FTIR spectrum (Fig. S1b), the peak at 1607 cm^{-1} was attributed to C=N stretching, which demonstrated that imine groups formed in COF-V, COF-OH-SH, and COF-S-SH. The SEM results for COF-V (Fig. S2) showed strips of nanofibers, which was consistent with the previous report [36]. Additionally, the -OH-SH and -S-SH anchoring groups on the COF-V pore wall made the nanofiber surface rough (Fig. 2a and b).

To analyze the crystalline structure of COF-V, the powder XRD (PXRD) data were compared with the computational structural simulations and Pawley refinement. COF-V produced a substantial PXRD peak at 2.9° (Fig. 2c, black curve). Some weaker peaks were observed at 4.9°, 5.8°, 7.3°, and 23.4°, which were assigned to the (1 0 0), (1 1 0), (2 0 0), (2 1 0), and (0 0 1) diffractions, respectively. These results were consistent with the previous report [36]. To study the geometrical structure, Pawley refinements were used to simulate the theoretical PXRD pattern. The mainly characteristic peaks are shown in Fig. 2c (observed reflections). The fitted curve (Fig. 2c, black and dark blue lines) showed excellent agreement with the experimentally observed pattern, and exhibited a negligible difference (Fig. 2c, green line) with a very low weighted full spectrum factor (R_{WP}, 2.68%) and full spectrum factor (R_P, 2.01%). A structural model of the COF-V framework was built. The PXRD pattern (Fig. 2c, violet curve) of the AA stacking mode almost reproduced the experimental and Pawley refinement patterns. Moreover, the apparent facet of (0 0 1) at 23.4° was assigned to a π-π stacking distance of 3.8 Å, which indicated that the stacking direction of COF-V extended perpendicular to the two-dimensional layers. The BET specific surface area (Fig. 2e) of COF-V calculated from the N_2 sorption isotherms at 77 K was 1204.6 $m^2\ g^{-1}$. The total pore volume of COF-V was 0.68 $cm^3\ g^{-1}$.

Because of the high crystallinity and mesoporous channels of COF-V, bis(2-mercaptoethyl) sulfide and dithiothreitol were artificially grafted onto COF-V as flexible chains. This gave efficient Hg(II) removal due to the introduction of thioether and thioalcohol groups. The PXRD patterns of COF-S-SH (blue curve) and COF-OH-SH (red curve) retained most of the COF-V peaks (Fig. 2c), especially the peaks at the facet of (0 0 1). However, the appearance of burrs and weak blue shift was attributed to the introduction of large numbers of flexible chains on the pores of COF-V matrix. Additionally, the BET specific surface area of COF-V was 1204.6 $m^2\ g^{-1}$ higher than that in the previous report [36]. The COF-S-SH and COF-OH-SH also exhibited high BET surface areas of 814.8 and 720.3 $m^2\ g^{-1}$, respectively. The total pore volumes of COF-S-SH and COF-OH-SH were 0.49 and 0.44 $cm^3\ g^{-1}$, respectively, which showed that the pore accessibility was maintained after modification. In the structures of COF-V and the two modified COFs, the lengths of -CH=CH_2, -CH_2-CH_2-S-CH_2-CH_2-S-CH_2-CH_2-SH, and -CH_2-CH_2-S-CH_2-CH(OH)-CH(OH)-CH_2-SH were approximately 3.1,

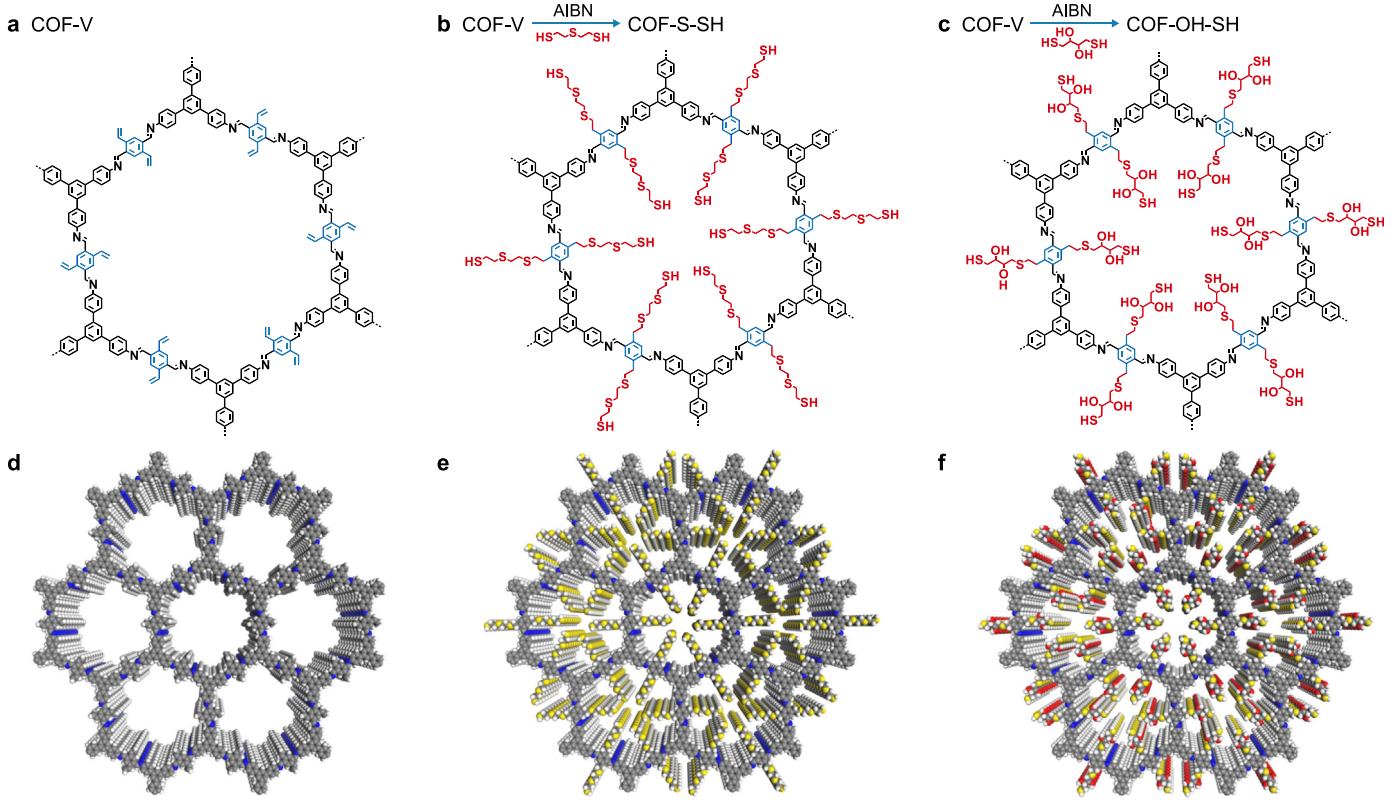

Fig. 1. a, The molecular configuration of COF-V. **b**–**c**, Synthetic scheme for production of COF-S-SH (**b**) and COF-OH-SH (**c**) through modification of COF-V. **d**–**f**, Top view of the AA stacking structure of COF-V (**d**), COF-S-SH (**e**), and COF-OH-SH (**f**).

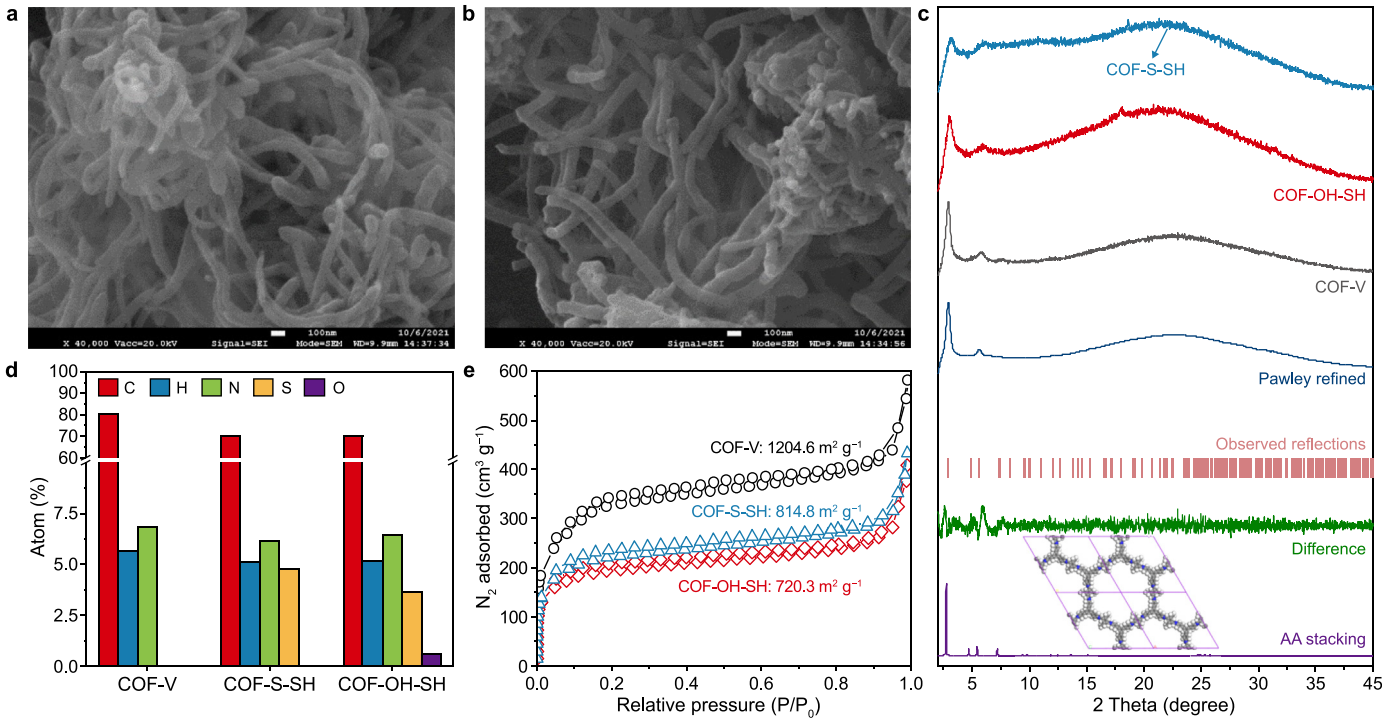

Fig. 2. **a**–**b**, SEM images of COF-OH-SH (**a**) and COF-S-SH (**b**). **c**, XRD profiles of COF-V (black), COF-OH-SH (red), COF-S-SH (blue), the Pawley refined (dark blue and pink lines), and predicted AA stacking structure of COF-V (violet). **d**–**e**, Elemental composition (**d**) and nitrogen adsorption (**e**) isotherm curves for the three COFs.

12.0, and 9.6 Å, respectively. These results showed that the two

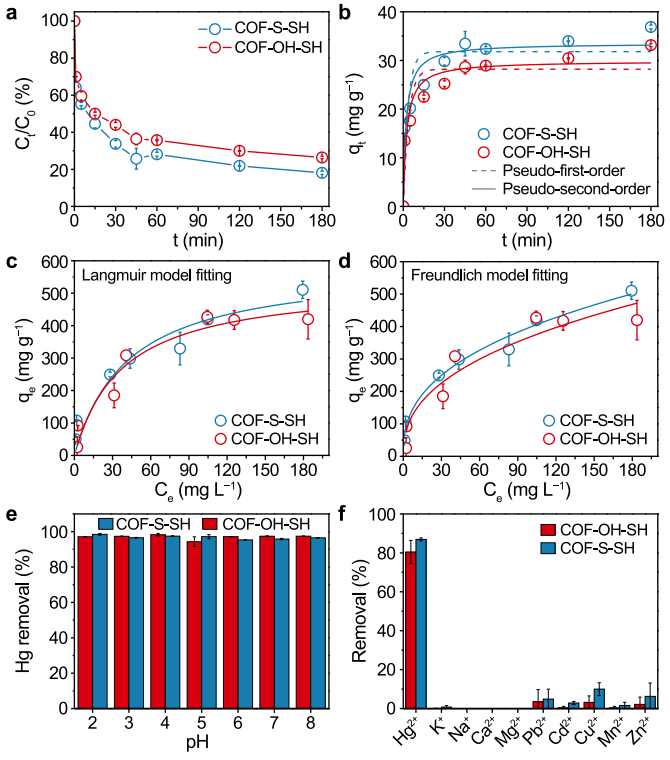

Fig. 3. a–**b**, Hg(II) adsorption kinetics (**a**) and fitting by pseudo-first- and second-order kinetic models (**b**). **c**–**d**, Hg(II) adsorption isotherms fitted by Langmuir (**c**) and Freundlich (**d**) adsorption models. **e**, Hg(II) adsorption in solutions with different pH values. **f**, Hg(II) adsorption in solutions containing a mixture of metal ions.

modified groups were much longer than the -CH=CH_2 group. This might cause blocking of some of the micro-pores (with ø < 1.0–2.0 nm), which would decrease the BET specific surface areas of the modified COFs. The morphologies of COFs were observed by SEM, COF-S-SH and COF-OH-SH also showed a similar shape with COF-V, indicating that the introduction of groups has rarely changed the morphology of COF-V.

3.2. Adsorption of Hg(II) on the COFs

The prepared COF-S-SH and COF-OH-SH were applied to remove Hg(II) from water. The removal efficiencies of Hg(II) using COF-S-SH and COF-OH-SH were about 80% (Fig. 3a). The obvious Hg 4f peaks were determined in the XPS spectrums of two COFs after adsorbing Hg(II) (Fig. S3) and further affirmed the occurrence of the adsorption process. To further reveal the adsorption process, first- and second-order kinetic models were used to fit the experimental data. The results (Fig. 3b and Table S2) showed that the second-order model better described the Hg(II) adsorption kinetics ($R^2 > 0.92$). This indicated that the adsorption process of Hg(II) onto two functional COFs might be predominantly dominated by chemisorption via Hg(II) binding/chelating with -SH groups [37,47]. In addition, the adsorption rate for COF-S-SH and COF-OH-SH adsorbing Hg(II) was calculated by the second-order model with v_0 (Table S2) of 15.94 and 12.22 mg g^{-1} min^{-1}, respectively. These results indicated that COF-S-SH had a faster adsorption rate than COF-OH-SH for Hg(II). This difference might be ascribed to the electrostatic potential distribution (Fig. S4) with the introduction of a hydroxyl group affecting the electronegativity around the S atom.

Adsorption isotherms were used to investigate the maximum Hg(II) adsorption capacities of the modified COFs. Langmuir and Freundlich's models were used to fit the experimental data. Increasing the Hg(II) concentration in the adsorption system almost simultaneously enhanced the adsorption capacities of COF-S-SH

and COF-OH-SH for Hg(II) removal (Fig. 3c and d). In addition, according to the Langmuir isotherm model, the maximum adsorption capacities of Hg(II) on COF-S-SH and COF-OH-SH were 586.3 and 535.5 mg g^{-1}, respectively. The adsorption capacities of the prepared COFs were approximately equal to that of a COF prepared in a previous study (COF-TABPB-S-SH) [38] and higher than those of conventional adsorbents [37,48,49]. Interestingly, the two post-synthetically modified COFs had different adsorption isotherm curves and fitting parameters (Table S3). In the case of COF-S-SH, the experimental data were fitted well by the Freundlich model ($R_F^2 > R_L^2$) with a low value of $1/n$ (0.388). This confirmed that the structure with two thioethers (-S-) and a thiol (-SH) might participate in the multilayer adsorption process [50,51] and that the adsorption proceeded readily [52,53]. For COF-OH-SH, the Langmuir and Freundlich models showed similar fitting results for Hg(II) adsorption. The contribution of -OH on COF-OH-SH to Hg(II) adsorption was not as apparent as that of -S- for Hg(II) adsorption on COF-S-SH because the Langmuir model predicts uniform adsorption [54]. The Hg(II) adsorption capacities of the prepared COFs and other adsorbents were compared (Table S4). Introduction of functional groups (-SH or $-NH_2$) obviously improved the Hg(II) adsorption capacity compared with other adsorbents. This comparison highlighted the benefits of optimizing the structure and pre-designing functional groups in COFs. Thus, the superiority of covalent organic frameworks in flexibility and modularity will promote its deep application in various fields.

The solution pH is a critical factor in the adsorption process as it affects the adsorbent and adsorbate surface chemistry [51]. The effects of pH values between 2 and 8 on the post-synthetically modified COFs were investigated (Fig. 3e). The results displayed that both COFs performed remarkably consistent in removing Hg(II) from water over a wide pH range. This might be due to the strong binding/chelating interaction between sulfur and Hg(II), which would form stable adsorption configurations [38]. This is essential for selecting and applying suitable adsorbents in a complex environment to remove the target pollutants. Both of the post-synthetically modified COFs exhibited better removal efficiencies for Hg(II) than other metal ions in a mixed solution containing ten metal cations (Fig. 3f). These results indicated that the thiol group showed an excellent affinity for Hg(II) [55]. Thus, the outstanding selectivity assured the potential application of these two post-synthetical COFs in environmental remediation.

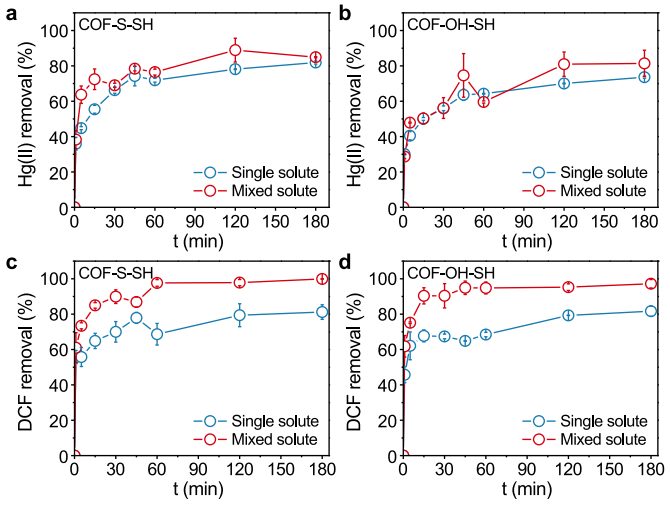

Fig. 4. Competitive adsorption kinetics between Hg(II) (**a**, **b**) and DCF (**c, d**) on COF-S-SH and COF-OH-SH.

3.3. Adsorption of Hg(II) with a co-existing anionic organic pollutant

The adsorption kinetics of Hg(II) on the two modified COFs were investigated in a mixed bisolute system containing Hg(II) and diclofenac sodium (DCF) (Fig. 4). It was interesting that the adsorption amount of Hg(II) on both COFs in the bisolute system was slightly higher than that in the single Hg(II) solute. Meanwhile, the adsorption of DCF on both two COFs in the bisolute system considerably significantly than that in the single DCF solute. Compared with the single-solute system, the bisolute system resulted in increases in the equilibrium removal rate of Hg(II) by approximately 3.0% and 7.78% for COF-S-SH and COF-OH-SH, respectively. In contrast, the equilibrium removal percentages of DCF in the bisolute system increased by approximately 18.17% and 15.54% for COF-S-SH and COF-OH-SH, respectively, compared with the single solute system. Additionally, adsorption equilibrium for DCF on COF-OH-SH was reached within 15 min in the bisolute system, which was much faster than for COF-S-SH. The anionic DCF could be bound by -OH groups on COF-OH-SH via electrostatic interactions [56]. Because of the synergistic chelation of Hg(II) and the -OH group, DCF adsorption on COF-OH-SH-Hg(II) was more rapid and higher than that on COF-S-SH-Hg(II).

To further clarify the synergistic adsorption behavior between Hg(II) and DCF, the adsorbates were adsorbed separately. First, one adsorbate was added to the adsorption system and the mixture was shaken for 30 min (pre-adsorption). Next, the other adsorbate was added (post-adsorption) to investigate the influence of the pre-adsorption process on post-adsorption of Hg(II) or DCF. Both pre-adsorption and post-adsorption enhanced the amounts of Hg(II) and DCF adsorbed on the modified COFs in the bisolute system (Fig. 5). Notably, the process of pre-adsorption of Hg(II) and then post-adsorption of DCF on two COFs showed a favorable tendency in enhancing the adsorption amount of Hg(II). While, the process of pre-adsorption of DCF and then post-adsorption of Hg(II) on two COFs were more favorable to improve the adsorption amount of DCF. These results suggest that the synergistic effect is more evident for the adsorbate with the faster adsorption rate. In the competitive system, the different sites of adsorbent were corresponding for adsorbing different adsorbates. DCF, with a quicker

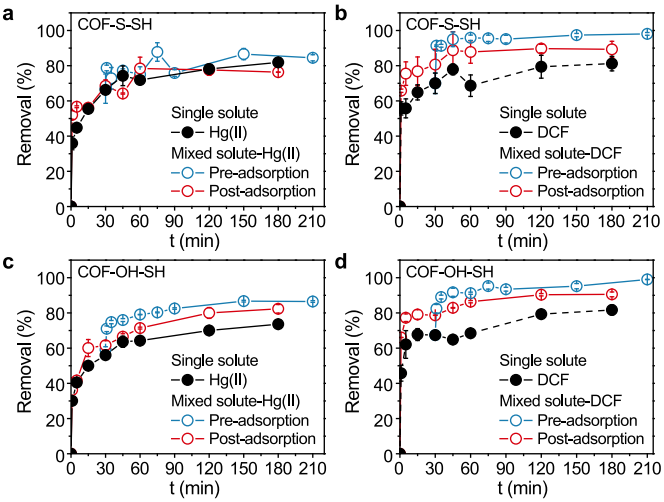

Fig. 5. Pre-adsorption and post-adsorption of Hg(II) (**a**, **c**) and DCF (**b**, **d**) on COF-S-SH and COF-OH-SH. For the mixed solute-Hg(II) with pre-adsorption, Hg(II) was adsorbed first for 30 min before DCF. For the mixed solute-Hg(II) with post-adsorption, DCF was adsorbed first for 30 min before Hg(II).

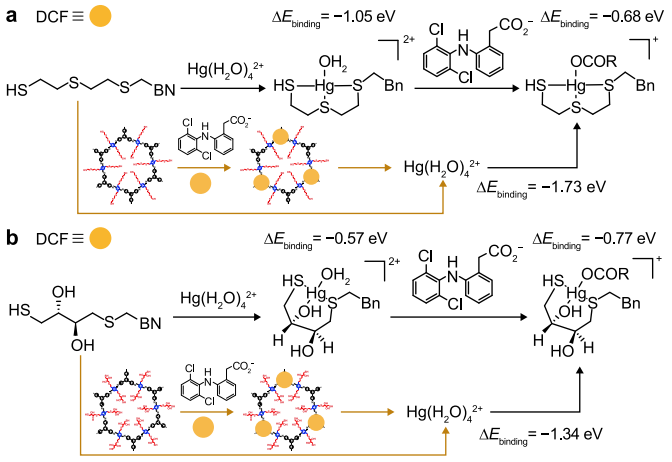

Fig. 6. The adsorption and calculated binding energies (Δ*E*) of Hg(II) on COF-S-SH (**a**) and COF-OH-SH (**b**), and the adsorbed Hg(II) or DCF as a new site for adsorbing another adsorbate in water. The structure of -OCOR representing anionic DCF. Bn is benzyl.

adsorption rate, will first occupy its effective adsorption site. Then, the adsorbate Hg(II) with a lower rate will also adsorb on its efficient adsorption site. Significantly, the adsorbed Hg(II) will then act as a new effective site for adsorption of anionic DCF in addition to the existing site in the COF, which will enhance the DCF adsorption. However, the pre-adsorbed DCF may diminish the pore size of COFs, which will negatively affect the diffusion of the subsequent Hg(II). These two aspects lead to a more apparent synergistic promotion of DCF adsorption with a fast adsorption rate compared with the single adsorption system.

Additionally, the water from WWTP (waste water treatment plant in Xining, China) was used to prepare the simulated solution containing the mixture of Hg(II) and DCF for investigating the adsorption performance of two COFs. The removal efficiencies of Hg(II) by COF-S-SH and COF-OH-SH were stable, but the removal of DCF was inhibited (Fig. S5). It might be reasoned that those other anionic co-containments in the water could be attracted by

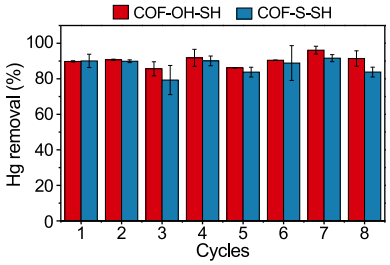

Fig. 8. Recycling performance of the two post-synthetic COFs for Hg(II) removal.

adsorbed Hg(II) or the positive H atom on the hydroxyl (-OH) for competing with DCF, and thus decrease the DCF removal.

3.4. Adsorption mechanism

To further explore the synergistic adsorption mechanism of Hg(II) and DCF on the COFs, the binding energies ($\Delta E_{binding}$) and frontier molecular orbitals were studied using Gaussian software. The $\Delta E_{binding}$ values of Hg(II) adsorbed on the COF-S-SH and COF-OH-SH models were −1.05 and −0.57 eV, respectively (Fig. 6). These values were in line with the result that COF-S-SH adsorbed more than COF-OH-SH. When the adsorbed Hg(II) being the available adsorption sites for anionic DCF, the $\Delta E_{binding}$ values for anionic DCF with COF-S-SH-Hg(II) and COF-OH-SH-Hg(II) were −0.68 and −0.77 eV, respectively. These results revealed that anionic DCF was easily adsorbed to Hg(II) sites on the COFs and that the adsorption process was exothermic. On the other hand, the $\Delta E_{binding}$ values of the synergistic adsorption of Hg(II) by COF-S-SH-DCF and COF-OH-SH-DCF were −1.73 and −1.34 eV, respectively. These values were much lower than those for Hg(II) adsorption on the two COFs. From Fig. 4, the enhanced adsorption of Hg(II) in the two bisolute systems was not apparent, indicating that synergistic adsorption was not commented for all the Hg(II) and DCF adsorption on COFs. Because of steric hindrance in the COFs channel, it might be difficult for DCF to approach Hg(II) on COFs.

The feasibility of the adsorption process can be evaluated

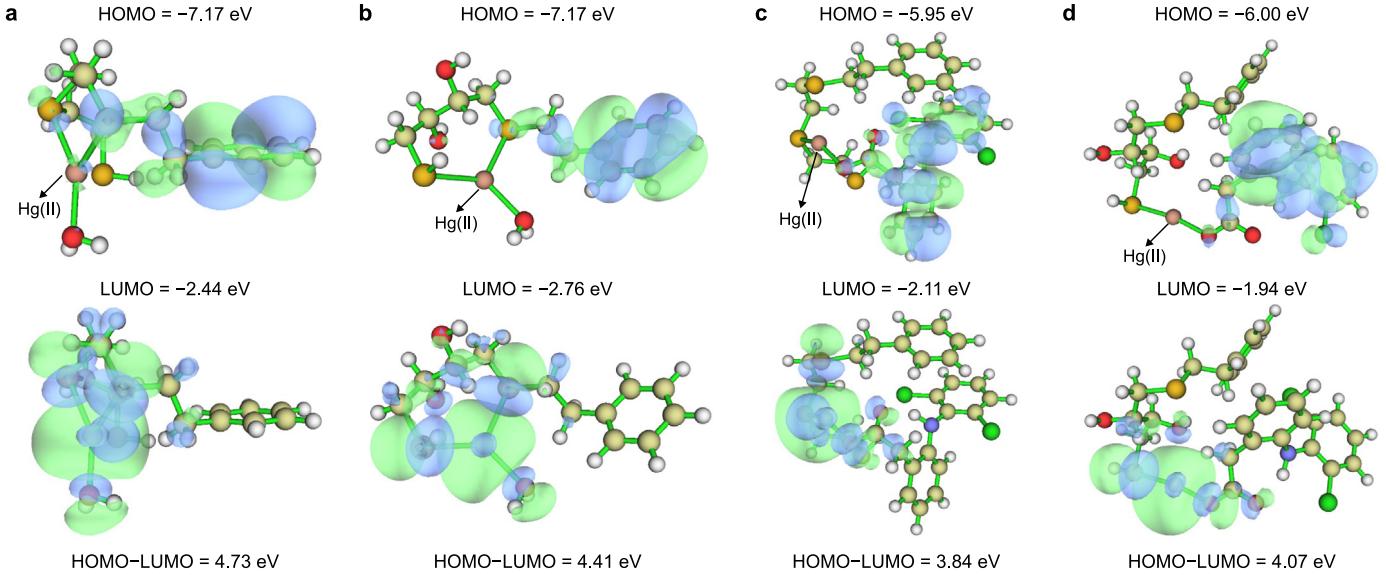

Fig. 7. HOMO and LUMO diagrams of COF-S-SH-Hg(II) (**a**), COF-OH-SH-Hg(II) (**b**), COF-S-SH-Hg(II)-DCF (**c**), and COF-OH-SH-Hg(II)-DCF (**d**), and the corresponding HOMO−LUMO energy gaps.

qualitatively and quantitatively using molecular orbitals [57], which can be obtained using Multiwfn software [58]. A high HOMO energy suggests strong electron donating capacity, while a low LUMO energy suggest a strong electron acceptance capacity. As shown in Fig. 7, the HOMO energy of COF-OH-SH-Hg(II) was the same as that of COF-S-SH-Hg(II). By contrast, its LUMO energy (−2.76 eV) was lower than that (−2.44 eV) of COF-S-SH-Hg(II). This result indicates COF-OH-SH-Hg(II) has a low HOMO-LUMO gap and more remarkable ability to accept electrons to its unoccupied orbitals. After DCF and Hg(II) were co-adsorbed on the two COFs, the HOMO surfaces were predominantly localized on the DCF molecules, which became the major electron donor atoms in the adsorption conjugates. Also, the adsorbed Hg(II) had a lower ability to accept electrons to its unoccupied orbitals and a more stable state after co-adsorption of DCF. This was evidenced by increased LUMO energies for the adsorption conjugate (COFs-Hg(II)-DCF) compared with the single Hg(II) solute system, which was still largely localized on Hg(II). Overall, the introduction of the strong electron donor DCF caused the HOMO-LUMO gap of DCF and Hg(II) co-adsorption conjugates to be lower than that of the single Hg(II) adsorption conjugates. These relatively unstable co-adsorption conjugates may be the main results for the unobvious adsorption promotion of Hg(II) in the bisolute system.

3.5. Reusability of COF-OH-SH and COF-S-SH

To investigate the reusability of the two COFs, Hg(II)-saturated COF-S-SH and COF-OH-SH were rinsed with an aqueous HCl solution (0.75 M). Then, the regenerated post-synthetic COFs were used in the next round of Hg(II) adsorption. As depicted in Fig. 8, COF-S-SH and COF-OH-SH maintained a stable efficiency with the Hg(II) removal percentage of 83.8% and 91.4% after eight cycles, respectively. It was interesting that a slight fluctuation was observed in the third and fifth cycles of reuse, which might be reasoned that these adsorbed Hg(II) was difficult to elute by the binding/chelating interaction of functional groups on the two COFs. Repeated elution might be help for releasing the adsorbed Hg(II) from the adsorption sites for a temporary and then re-occupied by those dissociative Hg(II) ions, resulting in the slight fluctuation. The Hg(II) concentration in the HCl eluent was measured, and not all of the adsorbed Hg(II) on the spent COFs was successfully desorbed, which further confirmed that the adsorption of Hg(II) fluctuated. Additionally, the characterization of SEM between before and after adsorbing Hg(II) onto these two COFs has been compared and the results showed in Fig. S6. It demonstrated that the physical and chemical structures of the two COFs did not change after the adsorption process, which further verified its stability during use. Thus, it would be a potentially effective strategy to pre-design [50] and post-introduce [36] thiols into the COFs matrix to solve the detection and remediation of Hg(II) pollution in the future.

4. Conclusions

The post-synthetical strategy was conducted to prepare the thiol-functionalized COFs (COF-S-SH and COF-OH-SH) based on the matrix of COF-V. XPS and elemental analysis results showed that the post-functionalization of COF-V was successful. The XRD results were consistent with those from theoretical simulations and indicated that the COF-V contained AA stacking. Both COF-S-SH and COF-OH-SH showed rapid adsorption and high adsorption capacities. The maximum adsorption capacities of COF-S-SH and COF-OH-SH for Hg(II) were 586.3 and 535.5 mg g^{-1}, respectively. The influence of solution pH on the adsorption capacities of COF-S-SH and COF-OH-SH was minimal. Excellent selectivity for Hg(II) was observed in water containing ten different cationic metal ions. Both COF-S-SH and COF-OH-SH were stable for reuse for Hg(II) removal, and removed 83.8% and 91.4% of Hg(II) after eight cycles, respectively. The co-existence of anionic DCF had a positive effect on Hg(II) adsorption on the two COFs, while the adsorbed Hg(II) also facilitated adsorption of anionic DCF. DFT calculations showed that co-adsorption of DCF on the two COFs facilitated stable Hg(II) adsorption. The adsorbed DCF could act as a binding site for adsorption of Hg(II) on the COFs.

Based on the conclusion of synergetic adsorption of Hg(II) and anionic DCF occurred on the prepared two COFs, the mode of interaction between various adsorbates in binary and multicomponent systems should be investigated in the future. Additionally, those used environmental materials might be the potential adsorbents for specific contaminant removal. Therefore, the deep utilization of adsorbents could be a popular method in environmental remediation.

CRediT authorship contribution statement

Wei Wang: Conceptualization, Investigation, Writing-original draft. **Min-Juan Gong:** Investigation. **Dong-Hai Zhu:** Funding acquisition. **Mohammadtaghi Vakili:** Writing-review & editing. **Zahra Gholami:** Writing-review & editing. **Huan-Huan Jang:** Methodology. **Shuang-Xi Zhou:** Supervision, Writing-original draft, Funding acquisition. **Han Qu:** Supervision, Writing-review & editing.

Declaration of competing interest

The authors declare that they have no known competing financial interests or personal relationships that could have appeared to influence the work reported in this paper.

Acknowledgments

This work was financially supported by the International Cooperation Project of Qinghai Province (Grant No. 2021-HZ-809) and the Key Youth Foundation of Qinghai University (Grant No. 2021-QGY-1). The authors would like to thank Shiyanjia Lab (www.shiyanjia.com) for the help of DFT calculation.

Appendix A. Supplementary data

Supplementary data to this article can be found online at https://doi.org/10.1016/j.ese.2023.100236.

References

[1] C. Jadán-Piedra, M. Baquedano, S. Puig, D. Vélez, V. Devesa, Use of Saccharomyces cerevisiae to reduce the bioaccessibility of mercury from food, J. Agric. Food Chem. 65 (13) (2017) 2876–2882.
[2] K. Liu, Q. Wu, S. Wang, D. Ouyang, Z. Li, D. Ding, G. Li, Y. Tang, L. Xiang, D. Han, M. Wen, T. Liu, L. Duan, H. Tian, J. Hao, Highly resolved inventory of mercury release to water from anthropogenic sources in China, Environ. Sci. Technol. 55 (20) (2021) 13860–13868.
[3] X.F. Hu, M. Lowe, H.M. Chan, Mercury exposure, cardiovascular disease, and mortality: a systematic review and dose-response meta-analysis, Environ. Res. 193 (2021), 110538.
[4] S. Guo, L. Zhang, Y. Dong, L. Gao, Y. Cao, X. Wei, L. Liang, Evaluation of mercury removal efficiency of coal through solvent extraction procedures, Energy Fuel. 33 (9) (2019) 8145–8150.
[5] X. Yan, P. Li, X. Song, J. Li, B. Ren, S. Gao, R. Cao, Recent progress in the removal of mercury ions from water-based MOFs materials, Coord. Chem. Rev. 443 (2021), 214034.
[6] H. Albatrni, H. Qiblawey, M.H. El-Naas, Comparative study between adsorption and membrane technologies for the removal of mercury, Separ. Purif. Technol. 257 (2021), 117833.
[7] S. Rajendran, A.K. Priya, P. Senthil Kumar, T.K.A. Hoang, K. Sekar, K.Y. Chong, K.S. Khoo, H.S. Ng, P.L. Show, A critical and recent developments on adsorption technique for removal of heavy metals from wastewater-A review,

Chemosphere 303 (2022), 135146.
[8] K. Gai, A. Avellan, T.P. Hoelen, F. Lopez-Linares, E.S. Hatakeyama, G.V. Lowry, Impact of mercury speciation on its removal from water by activated carbon and organoclay, Water Res. 157 (2019) 600–609.
[9] Y. Kong, L. Wang, Y. Ge, H. Su, Z. Li, Lignin xanthate resin-bentonite clay composite as a highly effective and low-cost adsorbent for the removal of doxycycline hydrochloride antibiotic and mercury ions in water, J. Hazard Mater. 368 (2019) 33–41.
[10] S. Ullah, A.G. Al-Sehemi, M. Mubashir, A. Mukhtar, S. Saqib, M.A. Bustam, C.K. Cheng, M. Ibrahim, P.L. Show, Adsorption behavior of mercury over hydrated lime: experimental investigation and adsorption process characteristic study, Chemosphere 271 (2021), 129504.
[11] J. Wang, C. Chen, Biosorbents for heavy metals removal and their future, Biotechnol. Adv. 27 (2) (2009) 195–226.
[12] X. Feng, X. Ding, D. Jiang, Covalent organic frameworks, Chem. Soc. Rev. 41 (2012) 6010–6022.
[13] W. Wang, S. Deng, L. Ren, D. Li, W. Wang, M. Vakili, B. Wang, J. Huang, Y. Wang, G. Yu, Stable covalent organic frameworks as efficient adsorbents for high and selective removal of an Aryl-Organophosphorus flame retardant from water, ACS Appl. Mater. Interfaces 10 (36) (2018) 30265–30272.
[14] P.J. Waller, F. Gándara, O.M. Yaghi, Chemistry of covalent organic frameworks, Accounts Chem. Res. 48 (12) (2015) 3053–3063.
[15] J.W. Colson, W.R. Dichtel, Rationally synthesized two-dimensional polymers, Nat. Chem. 5 (6) (2013) 453–465.
[16] L. Chen, K. Furukawa, J. Gao, A. Nagai, T. Nakamura, Y. Dong, D. Jiang, Photoelectric covalent organic frameworks: converting open lattices into ordered donor-acceptor heterojunctions, J. Am. Chem. Soc. 136 (28) (2014) 9806–9809.
[17] M. Dogru, M. Handloser, F. Auras, T. Kunz, D. Medina, A. Hartschuh, P. Knochel, T. Bein, A photoconductive Thienothiophene-Based covalent organic framework showing charge transfer towards included fullerene, Angew. Chem. Int. Ed. 52 (10) (2013) 2920–2924.
[18] S. Jin, M. Supur, M. Addicoat, K. Furukawa, L. Chen, T. Nakamura, S. Fukuzumi, S. Irle, D. Jiang, Creation of superheterojunction polymers via direct polycondensation: segregated and bicontinuous donor-acceptor π-Columnar arrays in covalent organic frameworks for Long-Lived charge separation, J. Am. Chem. Soc. 137 (24) (2015) 7817–7827.
[19] M. Calik, F. Auras, L.M. Salonen, K. Bader, I. Grill, M. Handloser, D.D. Medina, M. Dogru, F. Löbermann, D. Trauner, A. Hartschuh, T. Bein, Extraction of photogenerated electrons and holes from a covalent organic framework integrated heterojunction, J. Am. Chem. Soc. 136 (51) (2014) 17802–17807.
[20] A.F.M. EL-Mahdy, Y. Hung, T.H. Mansoure, H. Yu, Y. Hsu, K.C.W. Wu, S. Kuo, Synthesis of [3 + 3] β-ketoenamine-tethered covalent organic frameworks (COFs) for high-performance supercapacitance and CO_2 storage, J. Taiwan Inst. Chem. Eng. 103 (2019) 199–208.
[21] T. Joshi, C. Chen, H. Li, C.S. Diercks, G. Wang, P.J. Waller, H. Li, J.L. Bredas, O.M. Yaghi, M.F. Crommie, Local electronic structure of molecular heterojunctions in a single-layer 2D covalent organic framework, Adv. Mater. 31 (3) (2019), 1805941.
[22] Q. Gao, X. Li, G. Ning, H. Xu, C. Liu, B. Tian, W. Tang, K.P. Loh, Covalent organic framework with frustrated bonding network for enhanced carbon dioxide storage, Chem. Mater. 30 (5) (2018) 1762–1768.
[23] S. Wang, Q. Wang, P. Shao, Y. Han, X. Gao, L. Ma, S. Yuan, X. Ma, J. Zhou, X. Feng, B. Wang, Exfoliation of covalent organic frameworks into Few-Layer Redox-Active nanosheets as cathode materials for Lithium-Ion batteries, J. Am. Chem. Soc. 139 (12) (2017) 4258–4261.
[24] H. Furukawa, O.M. Yaghi, Storage of hydrogen, methane, and carbon dioxide in highly porous covalent organic frameworks for clean energy applications, J. Am. Chem. Soc. 131 (25) (2009) 8875–8883.
[25] L.G. Ding, S. Wang, B.J. Yao, F. Li, Y.A. Li, G.Y. Zhao, Y.B. Dong, Synergistic antibacterial and anti-inflammatory effects of a drug-loaded self-standing porphyrin-COF membrane for efficient skin wound healing, Adv. Healthc. Mater. 10 (8) (2021), 2001821.
[26] Q. Wang, H. Wang, L. Wang, L. Bai, C. Yang, T. Zhu, Porous graphene oxide functionalized by covalent organic framework for the application in adsorption and electrochemical: the effect of C-F bonds to structure, Microchem. J. 170 (2021), 106710.
[27] K. Zhao, P. Gong, J. Huang, Y. Huang, D. Wang, J. Peng, D. Shen, X. Zheng, J. You, Z. Liu, Fluorescence turn-off magnetic COF composite as a novel nanocarrier for drug loading and targeted delivery, Microporous Mesoporous Mater. 311 (2021), 110713.
[28] Q. Liu, S. Li, H. Yu, F. Zeng, X. Li, Z. Su, Covalently crosslinked zirconium-based metal-organic framework aerogel monolith with ultralow-density and highly efficient Pb(II) removal, J. Colloid Interface Sci. 561 (2020) 211–219.
[29] J. Chen, X. Tao, C. Li, Y. Ma, L. Tao, D. Zheng, J. Zhu, H. Li, R. Li, Q. Yang, Synthesis of bipyridine-based covalent organic frameworks for visible-light-driven photocatalytic water oxidation, Appl. Catal., B 262 (2020), 118271.
[30] S.K. Samanta, N. Dey, N. Kumari, D. Biswakarma, S. Bhattacharya, Multimodal ion sensing by structurally simple Pyridine-End Oligop-Phenylenevinylenes for sustainable detection of toxic industrial waste, ACS Sustain. Chem. Eng. 7 (14) (2019) 12304–12314.
[31] M. Afshari, M. Dinari, Synthesis of new imine-linked covalent organic framework as high efficient absorbent and monitoring the removal of direct fast scarlet 4BS textile dye based on mobile phone colorimetric platform, J. Hazard Mater. (2019), 121514.
[32] J. Wang, S. Zhuang, Covalent organic frameworks (COFs) for environmental applications, Coord. Chem. Rev. 400 (2019), 213046.
[33] W. Wang, Z. Zhou, H. Shao, S. Zhou, G. Yu, S. Deng, Cationic covalent organic framework for efficient removal of PFOA substitutes from aqueous solution, Chem. Eng. J. 412 (2021), 127509.
[34] D. Zhu, S. Zhou, Z. Zhou, R. Li, J. Ye, X. Ziyu, S. Lan, Y. Zhang, S. Miao, W. Wang, Highly efficient and selective removal of Cr(VI) by covalent organic frameworks: structure, performance and mechanism, Colloids Surf., A 600 (2020), 124910.
[35] N. Huang, L. Zhai, H. Xu, D. Jiang, Stable covalent organic frameworks for exceptional mercury removal from aqueous solutions, J. Am. Chem. Soc. 139 (6) (2017) 2428–2434.
[36] Q. Sun, B. Aguila, J. Perman, L.D. Earl, C.W. Abney, Y. Cheng, H. Wei, N. Nguyen, L. Wojtas, S. Ma, Postsynthetically modified covalent organic frameworks for efficient and effective mercury removal, J. Am. Chem. Soc. 139 (7) (2017) 2786–2793.
[37] Z. Yang, Y. Gu, B. Yuan, Y. Tian, J. Shang, D.C.W. Tsang, M. Liu, L. Gan, S. Mao, L. Li, Thio-groups decorated covalent triazine frameworks for selective mercury removal, J. Hazard Mater. 403 (2021), 123702.
[38] Y. Li, T. Hu, R. Chen, R. Xiang, Q. Wang, Y. Zeng, C. He, Novel thiol-functionalized covalent organic framework as adsorbent for simultaneous removal of BTEX and mercury (II) from water, Chem. Eng. J. 398 (2020), 125566.
[39] W. Wang, X. Mi, Z. Zhou, S. Zhou, C. Li, X. Hu, D. Qi, S. Deng, Novel insights into the competitive adsorption behavior and mechanism of per- and polyfluoroalkyl substances on the anion-exchange resin, J. Colloid Interface Sci. 557 (2019) 655–663.
[40] M.J. Frisch, G.W. Trucks, H.B. Schlegel, G.E. Scuseria, M.A. Robb, J.R. Cheeseman, G. Scalmani, V. Barone, G.A. Petersson, H. Nakatsuji, X. Li, M. Caricato, A.V. Marenich, J. Bloino, B.G. Janesko, R. Gomperts, B. Mennucci, H.P. Hratchian, J.V. Ortiz, A.F. Izmaylov, J.L. Sonnenberg, D. Williams-Young, F. Ding, F. Lipparini, F. Egidi, J. Goings, B. Peng, A. Petrone, T. Henderson, D. Ranasinghe, V.G. Zakrzewski, J. Gao, N. Rega, G. Zheng, W. Liang, M. Hada, M. Ehara, K. Toyota, R. Fukuda, J. Hasegawa, M. Ishida, T. Nakajima, Y. Honda, O. Kitao, H. Nakai, T. Vreven, K. Throssell, J.A. Montgomery, J.E. Peralta, F. Ogliaro, M.J. Bearpark, J.J. Heyd, E.N. Brothers, K.N. Kudin, V.N. Staroverov, T.A. Keith, R. Kobayashi, J. Normand, K. Raghavachari, A.P. Rendell, J.C. Burant, S.S. Iyengar, J. Tomasi, M. Cossi, J.M. Millam, M. Klene, C. Adamo, R. Cammi, J.W. Ochterski, R.L. Martin, K. Morokuma, O. Farkas, J.B. Foresman, D.J. Fox, Gaussian 09, Gaussian, Inc., Wallingford CT, 2013.
[41] R. Krishnan, J.S. Binkley, R. Seeger, J.A. Pople, Self-consistent molecular orbital methods. XX. A basis set for correlated wave functions, J. Chem. Phys. 72 (1) (1980) 650–654.
[42] S. Grimme, S. Ehrlich, L. Goerigk, Effect of the damping function in dispersion corrected density functional theory, J. Comput. Chem. 32 (7) (2011) 1456–1465.
[43] S. Grimme, J. Antony, S. Ehrlich, H. Krieg, A consistent and accurate *ab initio* parametrization of density functional dispersion correction (DFT-D) for the 94 elements H-Pu, J. Chem. Phys. 132 (15) (2010), 154104.
[44] D. Aravena, F. Neese, D.A. Pantazis, Improved segmented All-Electron relativistically contracted basis sets for the lanthanides, J. Chem. Theor. Comput. 12 (3) (2016) 1148–1156.
[45] F. Weigend, R. Ahlrichs, Balanced basis sets of split valence, triple zeta valence and quadruple zeta valence quality for H to Rn: design and assessment of accuracy, Phys. Chem. Chem. Phys. 7 (18) (2005) 3297.
[46] A.V. Marenich, C.J. Cramer, D.G. Truhlar, Universal solvation model based on solute electron density and on a continuum model of the solvent defined by the bulk dielectric constant and atomic surface tensions, J. Phys. Chem. B 113 (18) (2009) 6378–6396.
[47] J. Wang, X. Guo, Adsorption kinetic models: physical meanings, applications, and solving methods, J. Hazard Mater. 390 (2020), 122156.
[48] P.L. Yap, S. Kabiri, D.N.H. Tran, D. Losic, Multifunctional binding chemistry on modified graphene composite for selective and highly efficient adsorption of mercury, ACS Appl. Mater. Interfaces 11 (6) (2019) 6350–6362.
[49] B. Zhang, J. Li, D. Wang, M. Feng, X. Huang, Fast and effective decontamination of aqueous mercury by a highly stable zeolitic-like chalcogenide, Inorg. Chem. 58 (7) (2019) 4103–4109.
[50] S. Ding, M. Dong, Y. Wang, Y. Chen, H. Wang, C. Su, W. Wang, Thioether-Based fluorescent covalent organic framework for selective detection and facile removal of Mercury(II), J. Am. Chem. Soc. 138 (9) (2016) 3031–3037.
[51] L. Wu, C. Du, J. He, Z. Yang, H. Li, Effective adsorption of diclofenac sodium from neutral aqueous solution by low-cost lignite activated cokes, J. Hazard Mater. 384 (2020), 121284.
[52] S. Yang, S. Chen, Y. Chang, A. Cao, Y. Liu, H. Wang, Removal of methylene blue from aqueous solution by graphene oxide, J. Colloid Interface Sci. 359 (1) (2011) 24–29.
[53] J. Wang, X. Guo, Adsorption isotherm models: classification, physical meaning, application and solving method, Chemosphere 258 (2020), 127279.
[54] H. Ma, J. Yang, X. Gao, Z. Liu, X. Liu, Z. Xu, Removal of chromium (VI) from water by porous carbon derived from corn straw: influencing factors, regeneration and mechanism, J. Hazard Mater. 369 (2019) 550–560.
[55] G. Li, K. Zhang, P. Zhang, W. Liu, W. Tong, L. Hou, Y. Wang, Thiol-Functionalized pores via Post-Synthesis modification in a metal-organic framework with selective removal of Hg(II) in water, Inorg. Chem. 58 (5) (2019) 3409–3415.

[56] X. Mi, S. Zhou, Z. Zhou, M. Vakili, Y. Qi, Y. Jia, D. Zhu, W. Wang, Adsorptive removal of diclofenac sodium from aqueous solution by magnetic COF: role of hydroxyl group on COF, Colloids Surf., A 603 (2020), 125238.
[57] I.H.S. Ribeiro, D.T. Reis, D.H. Pereira, A DFT-based analysis of adsorption of Cd^{2+}, Cr^{3+}, Cu^{2+}, Hg^{2+}, Pb^{2+}, and Zn^{2+}, on vanillin monomer: a study of the removal of metal ions from effluents, J. Mol. Model. 25 (9) (2019) 267.
[58] T. Lu, F. Chen, Multiwfn: a multifunctional wavefunction analyzer, J. Comput. Chem. 33 (2012) 580–592.